JGR Space Physics

RESEARCH ARTICLE
10.1029/2019JA027598

Key Points:
- Oscillatory motion of MSTIDs over Tromsø in the duskside is driven by high-latitude convection electric field
- The duskside MSTIDs over Tromsø propagate in the eastward direction during quiet geomagnetic conditions
- The westward turning of duskside MSTIDs over Tromsø invariably coincides with increase in the local X component of the magnetic field

Supporting Information:
- Supporting Information S1

Correspondence to:
S. Yadav,
sneha.yadav84@gmail.com

Citation:
Yadav, S., Shiokawa, K., Oyama, S., & Otsuka, Y. (2020). Multievent analysis of oscillatory motion of medium-scale traveling ionospheric disturbances observed by a 630-nm airglow imager over Tromsø. *Journal of Geophysical Research: Space Physics*, *125*, e2019JA027598. https://doi.org/10.1029/2019JA027598

Received 1 NOV 2019
Accepted 15 FEB 2020
Accepted article online 21 FEB 2020

Multievent Analysis of Oscillatory Motion of Medium-Scale Traveling Ionospheric Disturbances Observed by a 630-nm Airglow Imager Over Tromsø

Sneha Yadav[1,2], K. Shiokawa[1], S. Oyama[1,3,4], and Y. Otsuka[1]

[1]Institute for Space-Earth Environmental Research, Nagoya University, Nagoya, Japan, [2]Space Physics Laboratory, Vikram Sarabhai Space Center, Trivandrum, India, [3]Ionosphere Research Unit, University of Oulu, Oulu, Finland, [4]National Institute of Polar Research, Tachikawa, Japan

Abstract We present a comprehensive investigation on the propagation characteristics of duskside medium-scale traveling ionospheric disturbances (MSTIDs) using 630.0-nm airglow emissions over Tromsø (69.6°N, 19.2°E; magnetic latitude: 66.7°N). The unique points of our observation are (1) duskside MSTIDs primarily exhibited eastward motion under quiet conditions but turned to the westward direction associated with geomagnetic disturbances, (2) the westward moving MSTIDs again turned to the eastward direction when the geomagnetic disturbance ceased, (3) the turning of MSTIDs to the westward direction was invariably associated with an increase of the northward component of the magnetic field observed by the local ground-based magnetometers and with the equatorward expansion of the auroral oval, and (4) the Super Dual Auroral Radar Network convection maps revealed that the location of Tromsø was inside (outside) the duskside convection cell during the time of appearance of westward (eastward) moving MSTIDs. The average eastward and westward velocities of MSTIDs were ~25–80 and ~40–140 m/s, respectively. The Doppler shift measurement of the 630-nm airglow by a Fabry-Perot interferometer at Tromsø showed that northeastward winds were predominant during the appearance of eastward moving MSTIDs. These experimental evidences suggest that the oscillatory motion of MSTIDs over high latitudes is driven by the convection electric field. The MSTIDs tend to move eastward under geomagnetically quiet conditions but show westward motion under the influence of convection electric field associated with auroral activities in the duskside of two-cell convection pattern.

1. Introduction

Understanding the coupling between atmosphere, ionosphere, and magnetosphere serves as an area of fundamental research for the space weather physics. The high-latitude ionosphere (auroral and polar) serves an important region for such studies as it is directly connected with the magnetosphere, making it sensitive to even a small change in the magnetospheric activity. The high-latitude ionosphere is known for the existence of plasma structures of various scale sizes ranging from hundreds of kilometers to centimeters. The generation mechanism that are responsible for the formation of such structures can be of different origin: particle precipitation from the magnetosphere, plasma instability mechanisms, and neutral atmospheric dynamics (Fejer & Kelley, 1980; Keskinen & Ossakow, 1983). The relative importance of these sources in generating and affecting these structures depends on the geomagnetic conditions and location of the region with respect to the magnetospheric boundaries

Among several plasma structures, the medium-scale traveling ionospheric disturbances (MSTIDs) are particularly important because their source mechanism is associated with several processes viz., tropospheric convections, auroral activity, plasma precipitations in the polar ionosphere, polar vortex, and plasma instability processes (Hargreaves, 1992). MSTIDs are wave-like structures in the ionosphere with horizontal wavelengths of 100–1,000 km and periods of 15 min to 1 hr (Hocke & Schlegel, 1996; Hunsucker, 1982). The phenomenon of MSTIDs has been investigated extensively using a variety of equipment such as ionosondes (Amorim et al., 2011; Ssessanga et al., 2017), satellites beacon (Forbes et al., 2016; Garcia et al., 2016), airglow imagers (Makela et al., 2010; Shiokawa, Ihara, et al., 2003), Global Navigation Satellite Systems (Huang et al., 2018; Otsuka et al., 2013; Saito et al., 1998), and the high frequency (HF) radars (Bristow et al., 1994; Oinats et al., 2016). The 630.0-nm airglow all-sky images particularly stand out because of high spatial

resolution (less than 1 km) and ability of revealing the two-dimensional (2-D) structure of MSTIDs. The 630-nm airglow has an emission layer at 200–300 km, and it is excited by the interaction between atomic oxygen ions in the ionospheric *F* region and thermospheric molecular oxygen. Therefore, the 630-nm airglow intensity is a true indicator of *F* region plasma density and its height variations (Shiokawa, Mori, et al., 2012; Shiokawa et al., 2013).

The nighttime midlatitude MSTIDs, which are observed frequently at middle and low latitudes, have been investigated extensively (Figueiredo et al., 2018; Garcia et al., 2000; Huang et al., 2018; Kotake et al., 2007; Kubota et al., 2000; Makela et al., 2010; Martinis et al., 2010; Nishioka et al., 2009; Saito et al., 1998; Shiokawa, Ihara, et al., 2003; Sivakandan et al., 2019; Tsugawa et al., 2007, and references therein). These observations show that nighttime MSTIDs primarily have northwest-southeast (NW-SE) phase front and propagate southwestward in the Northern Hemisphere. These MSTIDs have been found to be electrified in nature (e.g., Narayanan et al., 2018; Saito et al., 1995; Shiokawa, Ihara, et al., 2003), and observations have demonstrated the mirror images of the MSTIDs in the conjugate hemisphere (Martinis et al., 2011; Otsuka et al., 2004; Shiokawa et al., 2005). The classical theory of atmospheric gravity waves (Hines, 1960) was unable to explain this preferred propagation direction of MSTIDs. The nighttime midlatitude MSTIDs are believed to be associated with the plasma instability mechanism known as the Perkins instability. Perkins (1973) pointed out that the north-south electric field or eastward neutral winds could disturb the equilibrium of the nighttime midlatitude *F* layer. The consequent perturbations in the ionospheric conductivity can allow the generation of polarization electric fields and an instability leading to the development of MSTIDs. The phase front of these MSTIDs is not aligned along the magnetic field like equatorial plasma bubbles but subtend a significant angle from the magnetic field lines (e.g., Garcia et al., 2000; Shiokawa, Ihara, et al., 2003). Since Perkins instability mechanism correctly estimates the alignment of the phase fronts in conductivity variations, it is considered as a prime mechanism responsible for triggering MSTIDs in midlatitude ionosphere. The linear growth rate of this instability is very small (in the order of 10^{-6}/s) to trigger the instability (Garcia et al., 2000; Makela & Otsuka, 2011), and therefore, some other seeding mechanism is required to reinforce its small growth rate. The simulation results of Yokoyama et al. (2009) and Yokoyama and Hysell (2010) demonstrated that the polarization electric fields driven by the neutral winds in the *E* region is essentially important for the development of MSTIDs as well as the seeding of NW-SE perturbation in the *F* region.

The observations of MSTIDs at high latitudes using all-sky imagers are difficult because of the hindrance caused by the bright aurora. Therefore, as compared to the low latitudes and midlatitudes, the imaging observations of MSTIDs at high latitudes are rather sparse. In fact, the limited results on the propagation characteristics of MSTIDs over high latitudes hindered the progress in our understanding on these dynamical structures. In addition, there exist several source mechanisms which can trigger the MSTIDs over high latitudes as compared to other latitudes. Therefore, the exact mechanism that leads to the generation of MSTIDs over high latitudes is still an elusive aspect. The first observation of high-latitude nighttime MSTIDs was reported by Kubota et al. (2011) in 630-nm airglow images at Fairbanks, Alaska. These MSTIDs were found to propagate predominantly in the southwestward direction and believed to be triggered by atmospheric gravity waves because the background horizontal neutral wind was mostly northward, restraining the Perkins instability. They surmised that the auroral activity seen in the northeast of Fairbanks could be the source for the atmospheric gravity waves. Shiokawa et al. (2013) carried out the first statistical study of high-latitude nighttime MSTIDs observed by 630-nm airglow images over Athabasca and Tromsø. They concluded that these MSTIDs are caused primarily by the Perkins instability; however, an additional source by atmospheric gravity waves from lower altitudes can also contribute.

The motion of high-latitude MSTIDs and their propagation characteristics during different background conditions is another elusive aspect of the MSTIDs. By using 630-nm airglow images, Shiokawa, Mori, et al. (2012) for the first time reported the change in the propagation direction (oscillatory motion) of nighttime MSTIDs which were observed to be associated with the auroral brightening. It is worth mentioning here that after this case study, which comprised of only one event during 2009, no observations showing this distinct oscillating motions of MSTIDs have been reported till date. Further, this study left us with several unanswered questions like (1) is it a one-time event and (2) under what conditions do the motion of MSTIDs attain oscillatory features. This calls for detailed investigation on the characteristics of high-latitude MSTIDs and its association with auroral brightening. The present study is an attempt to shed a light on

the above aspects, in addition to provide a systematic picture on the propagation characteristics of MSTIDs over high latitudes by using five duskside MSTID events.

2. Data and Methodology

The primary data set for the present study is the airglow imager (imager number 12), which is one of the Optical Mesosphere Thermosphere Imagers (Shiokawa et al., 1999, 2009) and has been operated in Tromsø since 10 January 2009. The imager has a 180° field-of-view fish-eye lens, six band-pass optical filters, and a thermoelectrically cooled CCD with 512 × 512 pixels. CCD images processed with 2 × 2 binning (finally combined to 256 × 256 pixels for an image) have been made to increase the signal to noise ratio. This camera has six band-pass filters that allowed measurement of airglow/auroral emissions at specific wavelengths: OI at 557.7 nm, OI at 630.0 nm, Na at 589.3 nm, OH bands at 720–910 nm, OI at 732.0 nm, and background at 572.5 nm. This study utilizes the 630-nm airglow images which were taken every 95 s with exposure time of 45 s by using a band-pass optical filter with a bandwidth of 1.59 nm. The absolute intensity of the 630 nm has been obtained by subtracting the image from the background continuum intensity of the sky which was monitored at 572.5 nm at every 15 min. The raw images are projected into an equidistant grid under assumption that the emission intensity has a peak at 250-km altitude. In order to identify wave structures in the 630-nm image clearly, the deviation images have been generated by subtracting 1-hr running averages. The deviations are calculated as $(I(t) - I_a(t))/I_a(t)$, where $I(t)$ and $I_a(t)$ are the airglow intensity measured at time t and the average intensity over $t \pm 30$ min, respectively, for each pixel of images (Shiokawa, Ihara, et al., 2003; Shiokawa, Mori, et al., 2012).

The propagation characteristics of MSTIDs over Tromsø have been investigated by analyzing 9-years of data, that is, from January 2010 to February 2018. It is worth mentioning that MSTIDs can be found in faint fluctuations of the airglow intensity, and thus, the camera operation mode requires moderately long exposure time (e.g., 45 s) and binning in a CCD during readout. It is challenging to find out the structures of MSTIDs at high latitudes owing to occasional saturation of the image count during appearance of aurora in the camera field of view. In addition, the exposure time was often found to be reduced to 10 s facilitating the study of auroral activity over Tromsø. With these restrictions, the total number of nights when the data were available to examine the presence of wave structures, if any, were only about 75. Out of these nights, we could identify only seven cases of apparent MSTID-type structures. In this study, we present five intriguing events of duskside MSTIDs. These events have been selected because they occurred in same time sector, that is, 15–20 UT (1730–2230 magnetic local time) and exhibited different propagation characteristics. The rest two events occurred in the midnight sector and were found to be weak for further analysis.

The ionospheric convection maps provided by the Super Dual Auroral Radar Network (SuperDARN) (Virginia Tech SuperDARN group, 2015) are also used to examine the relative location of Tromsø with respect to the two-cell convection pattern.

Horizontal wind velocities during the appearance of MSTIDs are derived from Fabry-Perot Interferometer (FPI) at Tromsø. This FPI, which is a part of Optical Mesosphere Thermosphere Imagers, has been operated at Tromsø since January 2009. It measures thermospheric wind by scanning the sky in five directions (north, south, east, west, and zenith). The FPI measurements used in this study were based on 630.0-nm wavelength and were made at the zenith angle of 15° with an exposure time of 9 s per direction. Measurements at optical wavelength of 557.7 nm were also made sequentially for deriving winds at E region heights, but such measurements are not the subject matter of the present study. The time resolution of wind vector measurement including exposure and data transfer time was 150 s. However, in order to increase the signal-to-noise ratio, original FPI spectral images were integrated in a post-analysis, and the time resolution of the wind data to make figures in this paper is about 50 min. Assuming that the emission intensity has a peak at 250-km altitude, the horizontal distance from the zenith to individual oblique directions (15°) is 67 km. The details about the instrument and technique to derive wind speed from the Doppler shift of the airglow emission measurement can be found in Shiokawa, Kadota, et al., 2003; Shiokawa, Otsuka, et al., 2012).

The magnetometer data at Tromsø (TRO; 69.6°N, 19.2°E; magnetic latitude: 66.7°N) and Abisko (ABK; 68.4°N, 18.8°E; magnetic latitude: 66.1°N) (Tanskanen, 2009) have been used to examine the variation of X component (northward component) magnetogram during the propagation of MSTIDs. Tromsø is the place of the camera, and Abisko is close to the place of MSTIDs appearance as presented later. In order to obtain

the perturbations caused by ionospheric currents, it is prerequisite to remove the geomagnetically quiet-time variations along with dominant Earth's magnetic field. The SuperMAG portal provides the baseline subtracted magnetometer data, which are free from daily variations and yearly trend (Gjerloev, 2012). The 1-min data of interplanetary magnetic field (IMF) B_y and B_z observed by the WIND satellite, and AU and AL indices were obtained from Space Physics Data Facility. The WIND satellite data, which can be downloaded from the CDA Web, are time shifted up to the nose of the bow shock.

3. Observations

3.1. The 630-nm Airglow Imaging

Figure 1 depicts the representative 630-nm images to show the occurrence of MSTIDs on 14 February 2018 (a), 27 November 2010 (b), 12 February 2018 (c), 12 December 2017 (d), and 5 December 2010 (e) along with their phase surfaces (highlighted by white dashed lines). These images are deviations from 1-hr running average. The X and Y axes in Figure 1 represent meridional and zonal relative distance, respectively, from the zenith of Tromsø. The uniqueness of the study is that all the five MSTID events correspond to the same time sector, that is, 15–20 UT (1730–2230 magnetic local time). Large deviations seen in the northern part of the images are attributed to auroral activities. Oblique structures seen in the southern part but characterized by lower deviations are signatures of the MSTIDs, which are scientific targets to be analyzed in this study. Most of the MSTIDs presented in Figure 1 are located far away from aurorae in the north, but a part of the poleward side of MSTIDs for event of 05 December 2010 (panel e) may invade into the aurora. This is an example of difficulty encountered to study MSTIDs over high latitudes as mentioned in section 2, and in this study, we will focus on MSTIDs that are clearly distinguished from aurorae and appear at far equator side of aurorae. Movies S1–S5 in the supporting information indicate motion of MSTIDs for these five events, showing their temporal and spatial variations. It is observed that MSTIDs orient primarily in the NW-SE direction for 14 February 2018 (panel a), 27 November 2010 (panel b), and 12 December 2017 (panel d) and in the northeast-southwest (NE-SW) direction for 5 December 2010 (panel e). However, on a few occasions and in some areas, the phase surface of MSTIDs is found to be aligned in random directions which are also highlighted by dashed white lines in Figure 1. It is observed that MSTIDs show change in the alignment of phase surface during initial and later phase of their propagation. For instance, during the event of 14 February 2018 (panel a; Movie S1), the MSTIDs exhibit north-south alignment and also displayed C-shaped structures in the initial phase of their propagation. These MSTIDs orient in the NW-SE during the later time. Similarly, the phase surface of MSTIDs during 12 February 2018 (panel c; Movie S3) showed alignment primarily in the north-south direction. However, these north- to south-oriented MSTIDs exhibited a tendency to be aligned in the NW-SE direction at the later time (after ~1745 UT; Movie S3). On 5 December 2010 (Movie S4), in addition to the NE-SW aligned MSTIDs, another set of MSTID-type structures were observed at the northern edge of the images. These additional MSTIDs aligned along the NW-SE direction, persistently propagated in the northeast direction, and appeared to merge with the aurora. Such MSTIDs are not the subject matter of the present study because of their plausible contamination by aurora. We have discussed only about the MSTIDs observed at the southern edge of the images. It is worth mentioning that all the events occurred during quiet to unsettled geomagnetic conditions with Ap index remained less than 15. This has provided us with a distinct opportunity to study the characteristics of high-latitude MSTIDs under various background conditions in the duskside. In order to investigate the motion of MSTIDs more clearly, the keograms have been generated. A keogram is a time sequence of airglow intensity variation in the east-west (zonal keogram) and north-south (meridional keogram) direction. In order to avoid disturbance caused by the aurora, the zonal keogram is constructed by stripping the slices of airglow images at 150-km south of Tromsø. The black horizontal and vertical dashed lines in Figure 1a highlight the baselines used to take the cross sections for making keograms of all the events. In the present case, the zonal (east-west) keogram demonstrates the east-west motion of MSTIDs, whereas meridional (north-south) keogram is mainly used for studying the auroral activity. In the following subsections, the detailed description on the propagation characteristics of MSTIDs for all the considered cases will be described.

3.1.1. Case 1: 14 February 2018

Figure 2 shows keograms for 14 February 2018 along with geomagnetic component and geomagnetic activity indices. Figures 2a and 2b depict the zonal keogram for 630-nm airglow intensity and its deviation from 1-hr

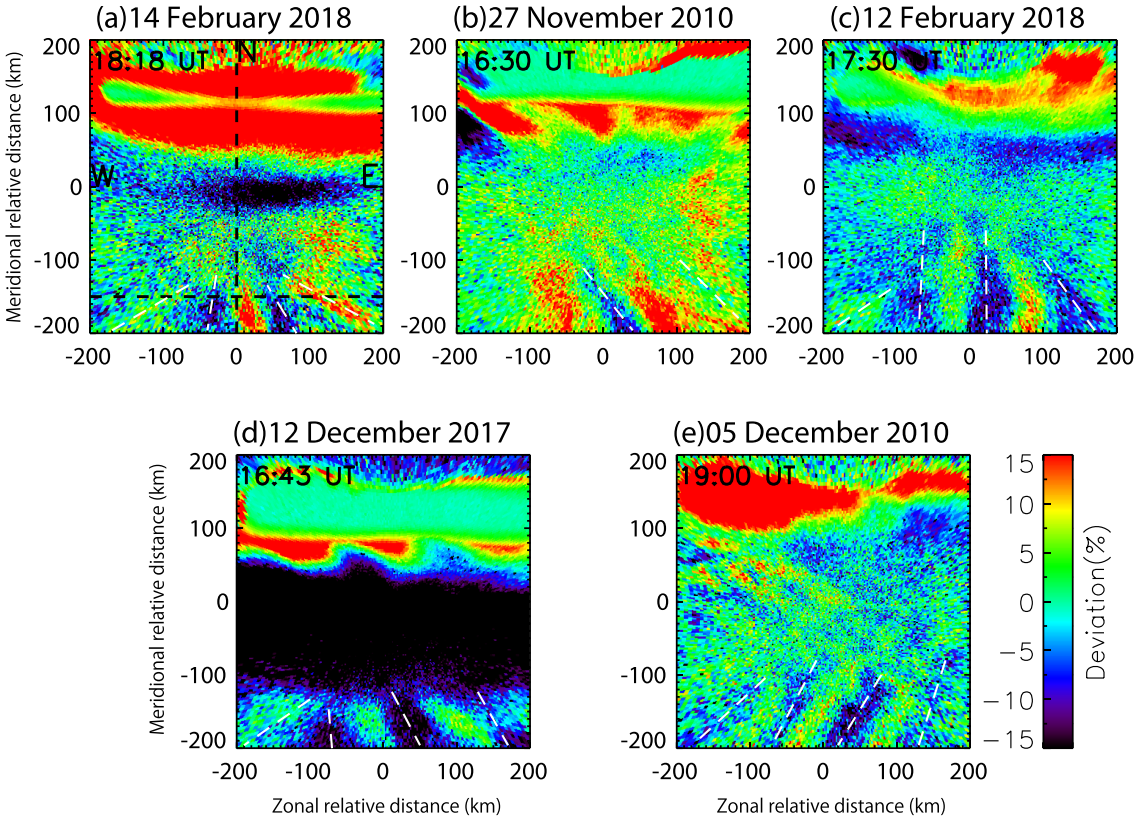

Figure 1. Examples of 630-nm images depicting the phase surface of the MSTIDs on 14 February 2018 (a), 27 November 2010 (b), 12 February 2018 (c), 12 December 2017 (d), and 5 December 2010 (e). The Y and X axes represent meridional and zonal relative distance, respectively, from the zenith of Tromsø.

running averages, respectively. The auroral activity can be seen in the meridional keogram presented in Figure 2c. The emission enhancement at ~1845 UT is due to contamination from artificial light. The increase in the 630-nm intensity toward the north of Tromsø represents the brightening of aurora. The presence of MSTIDs and its change in direction of propagation from eastward to westward are discernible from Figures 2a and 2b. The initially eastward (~30 m/s) moving MSTIDs began to move in the westward direction (~80 m/s) from ~1800 UT, and then they again reversed their motion and became eastward from ~1830 UT (45 m/s). The gradual equatorward expansion of the aurora was observed from 1800 UT. The aurora covered almost entire field of view of the imager after 1920 UT, causing saturation in the images. These MSTID and auroral variations can also be clearly seen in Movie S1.

In order to study the perturbations in the local magnetic field, the X component at Tromsø (TRO) and Abisko (ABK), which is located at a slightly lower latitude in the same magnetic meridian of Tromsø, are plotted in Figure 2d. The AU and AL indices, which represent eastward and westward ionospheric equivalent current, respectively, are depicted in Figure 2e. A small enhancement of ~4–5 nT starting from 1758 UT was observed in the X component at TRO and ABK coincided with westward turning of MSTIDs (highlighted by vertical dashed line). It should be noted that positive/negative values in the X component correspond to eastward/westward current in the *E* region. At ~1800–1830 UT, the X component at TRO continued to show perturbations with gradual increase but the X component values at ABK attained the negative values. The *AL* index also showed small but sudden decrease (in magnitude of about 100 nT) during 1800–1830 UT, suggesting the presence of small substorm-type activity. After this small substorm, the geomagnetic conditions appeared to be quiet during 1830–1900 UT. The *AL* index attained steady values of ~20 nT and X component at Tromsø showed a gradual fall during 1830–1900 UT. It is interesting to note that the MSTIDs again turned to the eastward direction after 1830 UT. The abrupt decrease in the *AL* index and sudden perturbations of relatively larger amplitudes in the X component at both stations appeared again after 19 UT, leading to the occurrence of intense aurora.

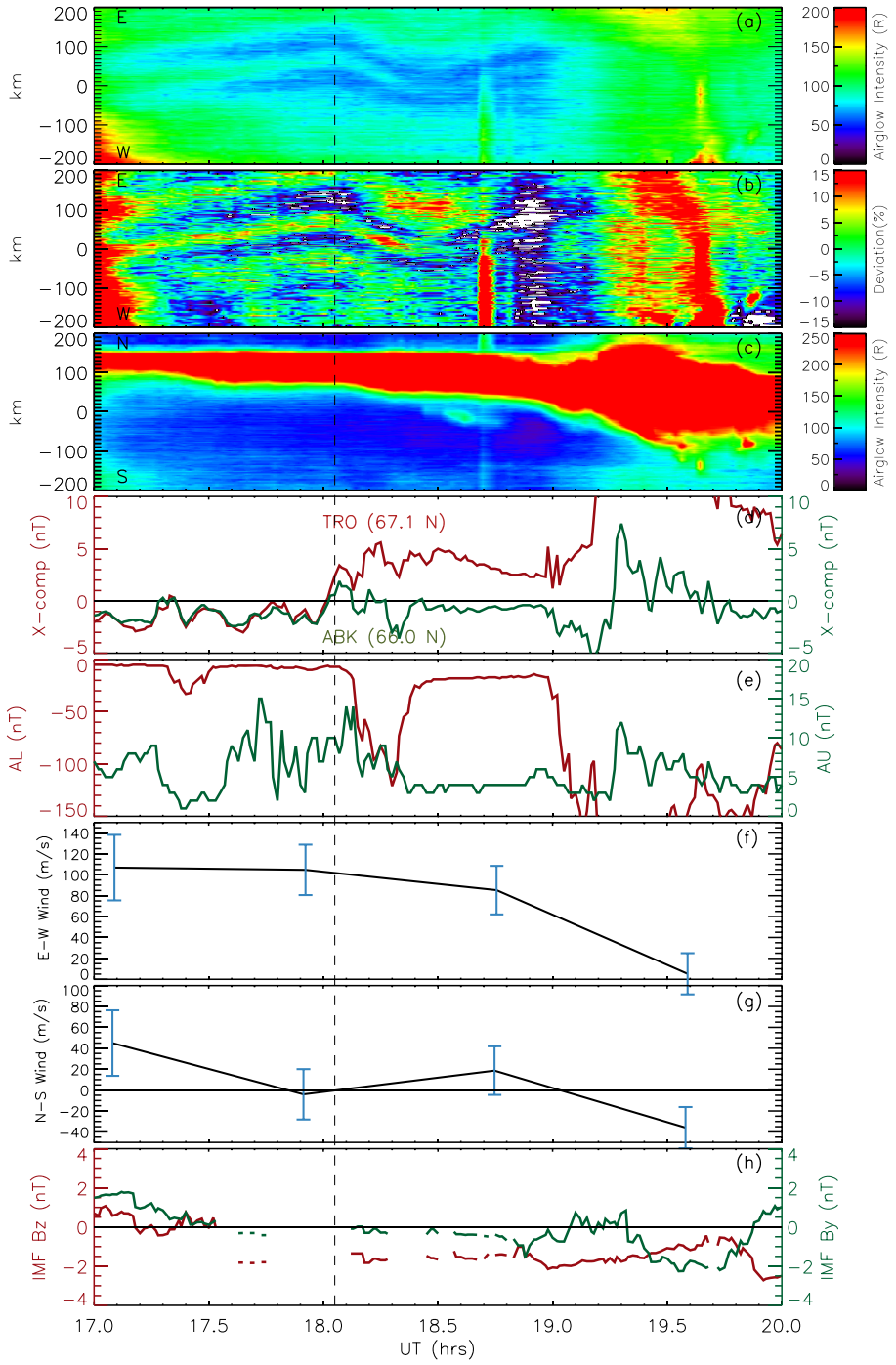

Figure 2. (a) East-west cross sections (keogram) of airglow images observed over Tromsø on 14 February 2018 for 630.0-nm intensity (b) and its deviations from 1-hr running averages. (c) North-south keogram of 630 nm emission intensity. (d) Variation of baseline subtracted X component of geomagnetic field at Tromsø (TRO) and Abisko (ABK). (e) Variation of *AU* and *AL*. (f) Variation of Eastward and Northward neutral wind speed observed by Fabry-Perot interferometer (FPI) derived through the Doppler shift of the 630-nm airglow. (h) Variation of IMF B_y and B_z components.

The eastward and northward neutral wind speed observed by FPI at Tromsø are depicted in Figures 2f and 2g, respectively. The relative location of the FPI scanning beam with respect to the aurora is crucial to understand the neutral dynamics in the MSTID region. At 1700 UT, the aurora appeared to be about 100 km away

from the zenith but its equatorward edge gradually expanded toward the equator and encompassed almost entire field of view of the imager after 1920 UT. The zonal wind remained dominantly in the eastward direction till 1800 UT with a magnitude of ~100 m/s, which is much faster than the eastward moving MSTIDs. Thereafter, the zonal wind showed gradual westward acceleration. The meridional wind showed oscillatory pattern, that is, it fluctuated between northward and southward direction. However, the meridional wind turned dominantly to the southward direction after ~1900 UT. Westward acceleration starting from 19 UT suggests that the thermosphere above Tromsø is driven by the sunward ionospheric convection, which is typically seen in the dusk, coinciding with equatorward expansion of the auroral oval due to increasing geomagnetic activity.

In order to access the interplanetary conditions, IMF B_z and B_y are shown in Figure 2h. It is predictable from the figure that IMF turned southward at ~1730 UT and remained southward throughout the considered time period without notable fluctuations.

3.1.2. Case 2: 27 November 2010

Figure 3 shows keograms of airglow images observed at Tromsø, X component of the magnetic field at TRO and ABK, and IMF B_y and B_z variation on 27 November 2010. The event of 27 November 2010 presents interesting motion of MSTIDs in east and west direction. They sequentially changed direction of motion and speed from ~1515 to ~1730 UT: eastward at ~40 m/s from ~1515 UT, westward at ~140 m/s from ~1545 UT, eastward at ~60 m/s from ~1610 UT, and westward from ~1650 UT at 30 m/s. The last westward motion was observed to abate at ~1700–1725 UT. The horizontal dashed-lines in Figure 3 highlight the time of westward reversal of MSTIDs. The 630-nm intensity of the aurora appeared to expand gradually southward from ~1500 UT to 1800 UT and, thereafter, covered the entire field of view. The MSTID and auroral variations can also be clearly seen in Movie S2.

The positive fluctuations in the X component at TRO and ABK during the time of westward turning of MSTIDs can be observed from Figure 3d. The first reversal of eastward moving MSTIDs in the westward direction at ~1750 UT coincided with the sharp positive fluctuation of about 7–10 nT in the X component at TRO and ABK. On the contrary, the AU/AL showed gradual decrease/increase during ~1500–1630 UT and, thus, exhibit no abrupt changes during the change in the MSTID propagation direction. It can be noted that during the eastward motion of MSTIDs at ~1615–1645, the X component at TRO and ABK mostly decreased with time. The X component at TRO and ABK, however, displayed a gradual increase from 1630 UT, and subsequently, MSTIDs again turned to westward direction from ~1655 UT. It is interesting to note that during the abatement of MSTIDs drift at ~1700–1725 UT, the X component at ABK exhibited almost constant values. The continuous decrease in the *AL* index and the southward expansion of aurora marked the presence of substorm after ~17 UT. Further, it is interesting to note that IMF B_z did not show any significant changes during the appearance of oscillatory motion of MSTIDs.

3.1.3. Case 3: 12 February 2018

Figure 4 shows keograms of airglow images observed at Tromsø, X component of the geomagnetic field at TRO and ABK, horizontal neutral wind at Tromsø, and IMF B_y and B_z variation for 12 February 2018. The MSTIDs propagate in the eastward direction from ~1710 UT with a phase speed of ~80 m/s. These eastward moving MSTIDs appeared to stagnate at ~1825–1835 UT (depicted by dashed line) before turning to westward direction. This stagnation and turning of MSTIDs occurred concomitantly with the enhancement in the X component of ~3 nT at TRO and ABK, and also with the sudden fluctuations in IMF B_z. It can be noted that aurora also gradually began to expand in the southward direction at 1825 UT and cover the entire field of view of the airglow imager after 1900 UT. The southward turning of IMF B_z from 1830 UT led to a small substorm activity, which is evident by the presence of negative bay of ~150 nT at ~1840 in the *AL* index. Thereafter, the *AL* index decreased continuously, displaying the presence of active geomagnetic conditions as also reflected in the X component magnetograms at both stations.

The zonal wind in Figure 4f was observed to be dominantly eastward and began to turn to westward direction after 1830 UT with increasing geomagnetic activity. The meridional wind was accelerated northward from 17 UT, remained northward till 18 UT (~20 m/s), and thereafter again accelerated to southward direction. The magnitude of the zonal wind speed was ~60 m/s during the time of appearance of eastward MSTIDs (~1730–1830 UT).

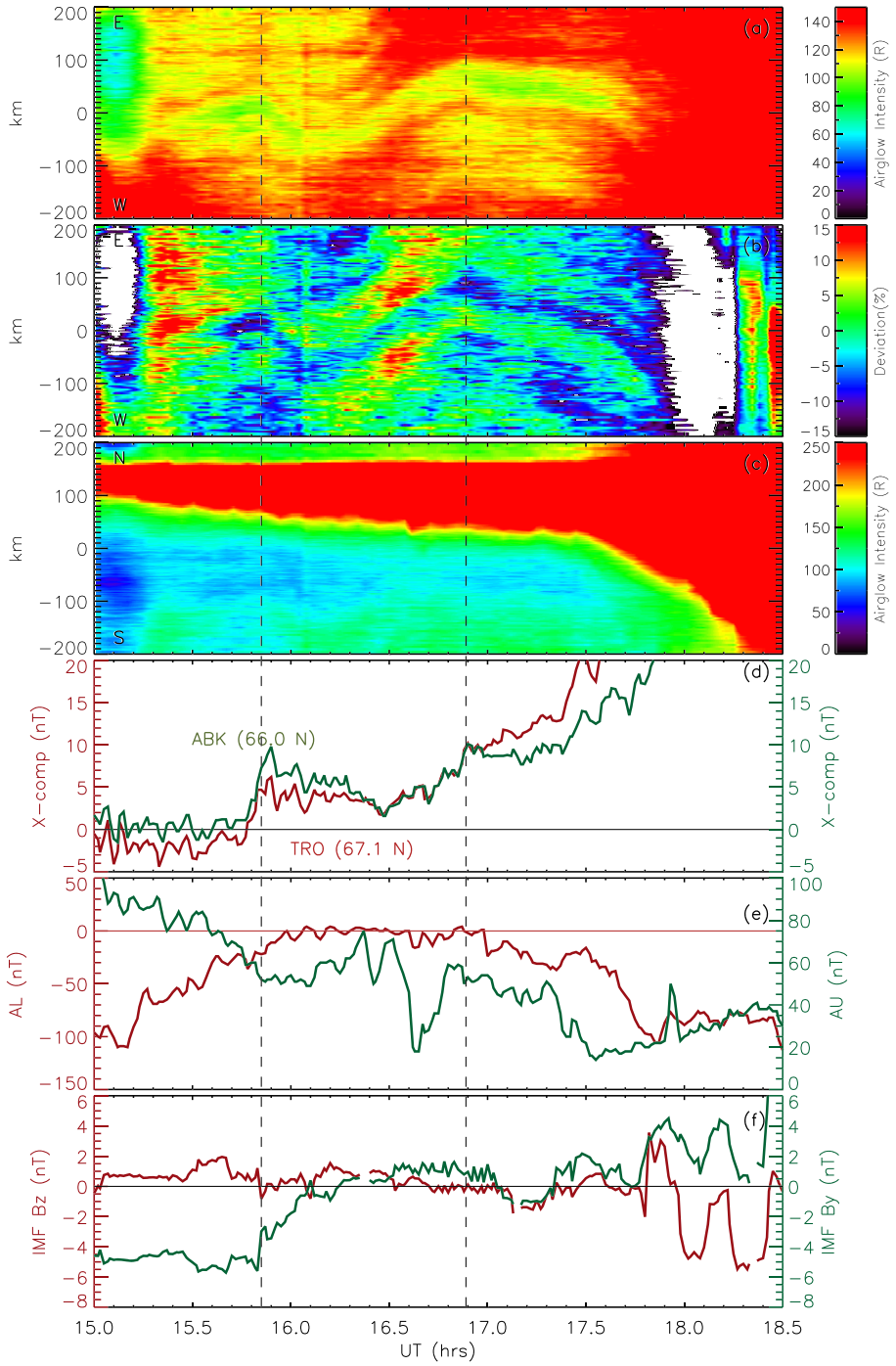

Figure 3. Same as Figure 2 but for 27 November 2010 and without neutral wind speed.

3.1.4. Case 4: 5 December 2010

The case of 5 December 2010, shown in Figure 5, has a unique feature characterized by persistent eastward propagation of MSTIDs from 1530 to 2030 UT. The continuous MSTID motion in the eastward direction can also be seen in Movie S4. These MSTIDs were found to move with a speed of ~25 m/s. The aurora started expanding southward gradually at ~18 UT and cover the entire field of view of the imager from ~2100 UT. The *AL* index showed the constant values of ~−20 nT during 15–20 UT, which approximately corresponds to time interval of eastward moving MSTIDs. A sharp decrease in the *AL* index after 2030 UT suggests the presence of the substorm type activity. The notable feature of this event is that although X component at

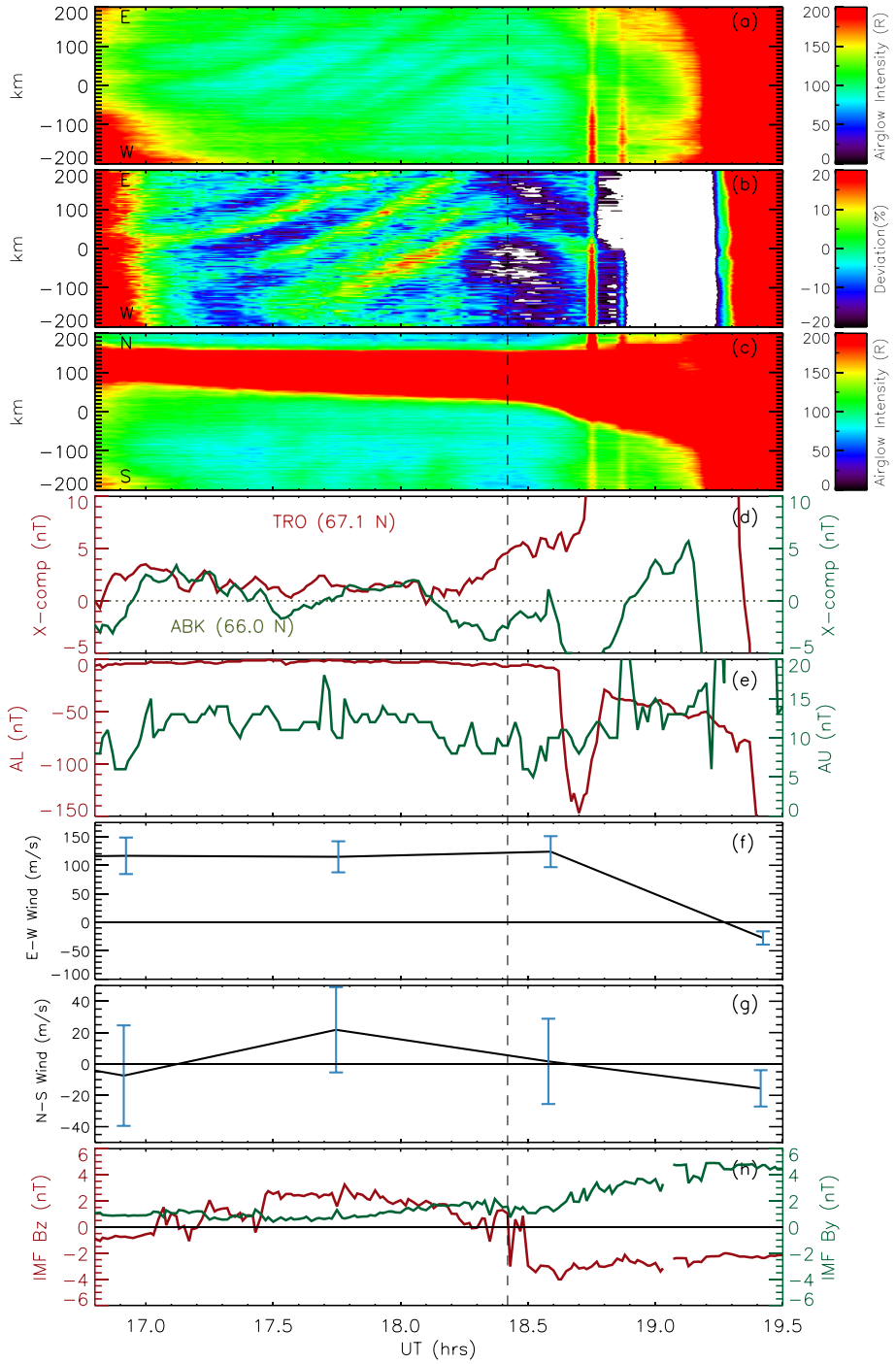

Figure 4. Same as Figure 2 but for 12 February 2018.

both the stations shows fluctuations during ~1500–2000 UT but no characteristic change is observed as noticed in the earlier cases.

3.1.5. Case 5: 12 December 2017

In contrast to the event of 5 December 2010, the MSTIDs propagate continuously in the westward direction for the event of 12 December 2017 as shown in Figure 6. The presence of aurora from the beginning of measurements, that is, from 1500 to 1600 UT can be seen from the figure. Unlike other events, the MSTIDs for this event was detected in the data from 1600 UT, after the brightening of aurora. Figure 6 also shows a

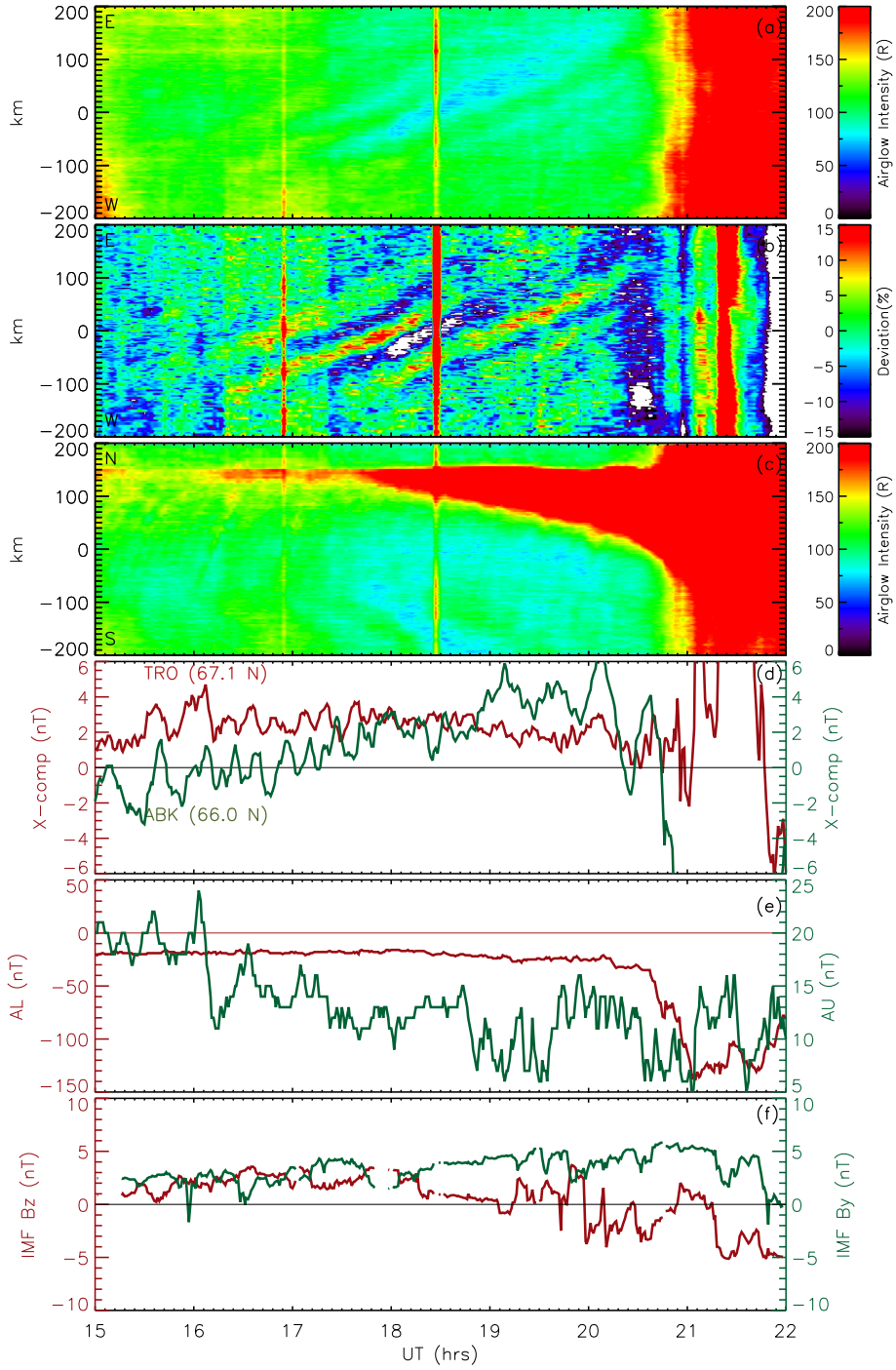

Figure 5. Same as Figure 2 but for 5 December 2010 and without neutral wind speed.

brightening in the southern sky at 1500–1615 UT which might be due to the presence of the auroral arc. These MSTIDs persistently move westward with a speed of ~105 m/s until 1630 UT. The retardation in this westward motion during ~1630–1700 UT is clear from Figure 6 and Movie S5. This decreased westward speed is estimated to be ~55 m/s at 1640–1700 UT. The X component magnetogram at both the stations displayed positive fluctuations of around 15 nT during ~1530–1700 UT and, thus, exhibit no characteristic change as observed in the previous cases during MSTIDs propagation. The IMF B_z

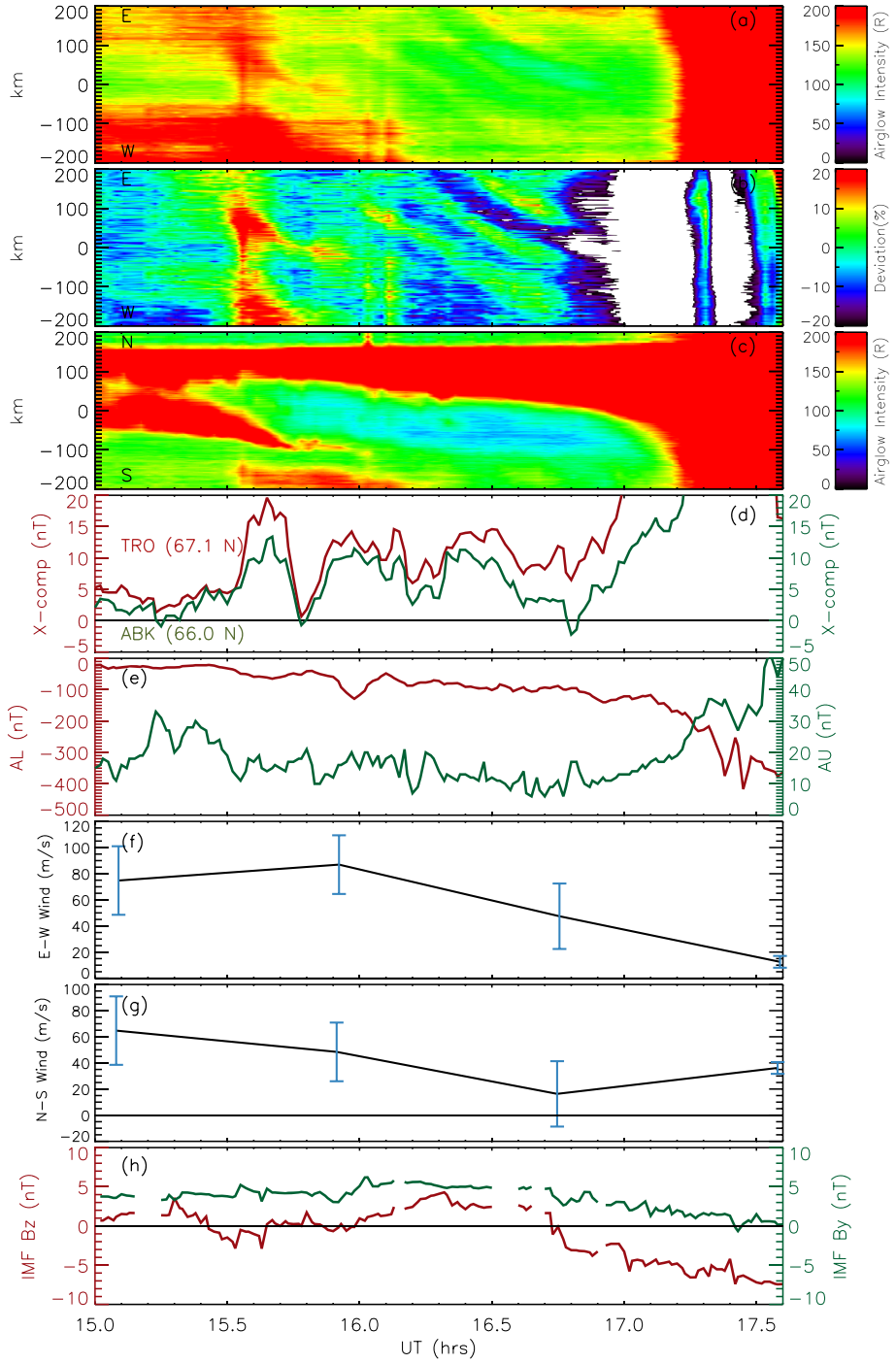

Figure 6. Same as Figure 2 but for 12 December 2017.

component became southward from 1645 UT. The abrupt decrease in the *AL* index after 1700 UT was followed by an intense aurora, suggesting the presence of a substorm. In spite of the brightening of aurora in the northern sky and auroral arc in the southern sky during ~1500–1600 UT, the zonal wind remained in the eastward direction, however with a considerably lesser magnitude (about ~75 m/s) as compared to the other two events of 2018 (100–125 m/s; Figures 2f and 4f). The zonal wind remained eastward throughout the considered time period, showed a maxima at ~1600 UT (~90 m/s), and then started to decrease. This westward acceleration occurred concomitantly with the southward expansion of aurora

seen at the northern part of the sky. The meridional wind remained in the northward direction throughout the event interval but its southward acceleration is clearly seen from ~1600 UT.

3.2. Convection Maps

The ionospheric plasma convection plays a key role to the dynamics of the *F* region at high latitudes. In order to examine the high-latitude ionospheric convection above the northern Scandinavia, convection maps estimated from the SuperDARN have been used in this study. Note that the convection pattern in the northern Scandinavian area was highly dependent on estimation from the standard map potential algorithm (Ruohoniemi & Baker, 1998) because of lack of measurements above the northern Scandinavia. There is thus likely inestimable ambiguity in determining the equator side edge of the convection pattern. We will thus refer to the convection map taking into account the magnetometer data shown in individual events. While we should have examined relative distance between the convection pattern and the MSTIDs area, the Tromsø site is adopted because of ambiguity of the convection pattern. The convection maps are available for events of 14 February 2018 (Figure 7), 12 February 2018 (Figure 8), and 12 December 2017 (Figure 9). The approximate location of Tromsø is depicted by red mark in the figures. The observation derived from these maps in context to the motion of MSTIDs are described as follows.

On 14 February 2018 (Figure 7), a quiet time convection pattern, which was restricted to high latitudes, can be seen at 1745 UT. Tromsø was situated well outside the high-latitude convection pattern. It can be noted from Figure 1 that during this time, the MSTIDs were moving in the eastward direction. However, as the time progressed, the auroral oval expanded owing to the increased geomagnetic activity (see the *AL* index shown in Figure 2e), suggesting changes in the high-latitude electric fields and currents. Tromsø was located at or inside the convection boundaries during the time when MSTIDs began to move in the westward direction. The auroral oval was found to contract and return to its initial state and Tromsø again appeared to be located well outside of the convection region at ~1900 UT. It is worthy of noting that westward moving MSTIDs again turned to the eastward direction from ~1830 UT.

Similarly, on 12 February 2018, during the time of eastward moving MSTIDs (at ~1730 UT), the prevalence of quiet geomagnetic conditions is reflected over high latitudes in terms of convection pattern being contracted to higher latitudes (see Figure 8). However, from ~1800 UT, gradual equatorward expansion of the auroral oval and the convection boundaries began to appear. It can be noted that MSTIDs also turned to the westward direction from 1830 UT.

The event of 12 December 2017 is different from the other events as the MSTIDs were found to propagate persistently in the westward direction. It is worthy of noting from Figure 9 that the auroral oval expanded equatorward well before the onset of MSTIDs. Tromsø was located well inside the convection boundaries during the appearance of westward moving MSTIDs in the dusk sector.

4. Discussion

The duskside MSTIDs observed in the 630-nm airglow emission over Tromsø were found to propagate primarily in the eastward direction under quiet geomagnetic conditions. These MSTIDs turned westward associated with commencement of geomagnetic disturbances and exhibited a tendency of turning to the eastward direction as the geomagnetic disturbance ceased. This distinctive pattern in the propagation of duskside MSTIDs over high-latitudes under various background conditions has not been reported yet and, therefore, is a matter of great interest. Even though the main intention of this paper is to investigate the propagation characteristics with background conditions under which MSTIDs oscillate, possible generation mechanisms of these MSTIDs have also been discussed in section 4.2 in order to have a comprehensive view of the phenomenon.

4.1. Propagation Characteristics of MSTIDs

Results reveal that the rapid change of MSTID propagation direction at high latitudes is caused by the prompt penetration of convection electric fields associated with magnetic disturbances. Observations clearly show that the rapid change in the propagation direction of MSTIDs from eastward to westward are directly related to local magnetic disturbances and auroral activity but not invariably linked to the global indices such as *Ap* and *AL*. The noteworthy feature of the present results is that the westward turning of MSTIDs invariably coincided with the enhancement in the horizontal component (X component) of the magnetic

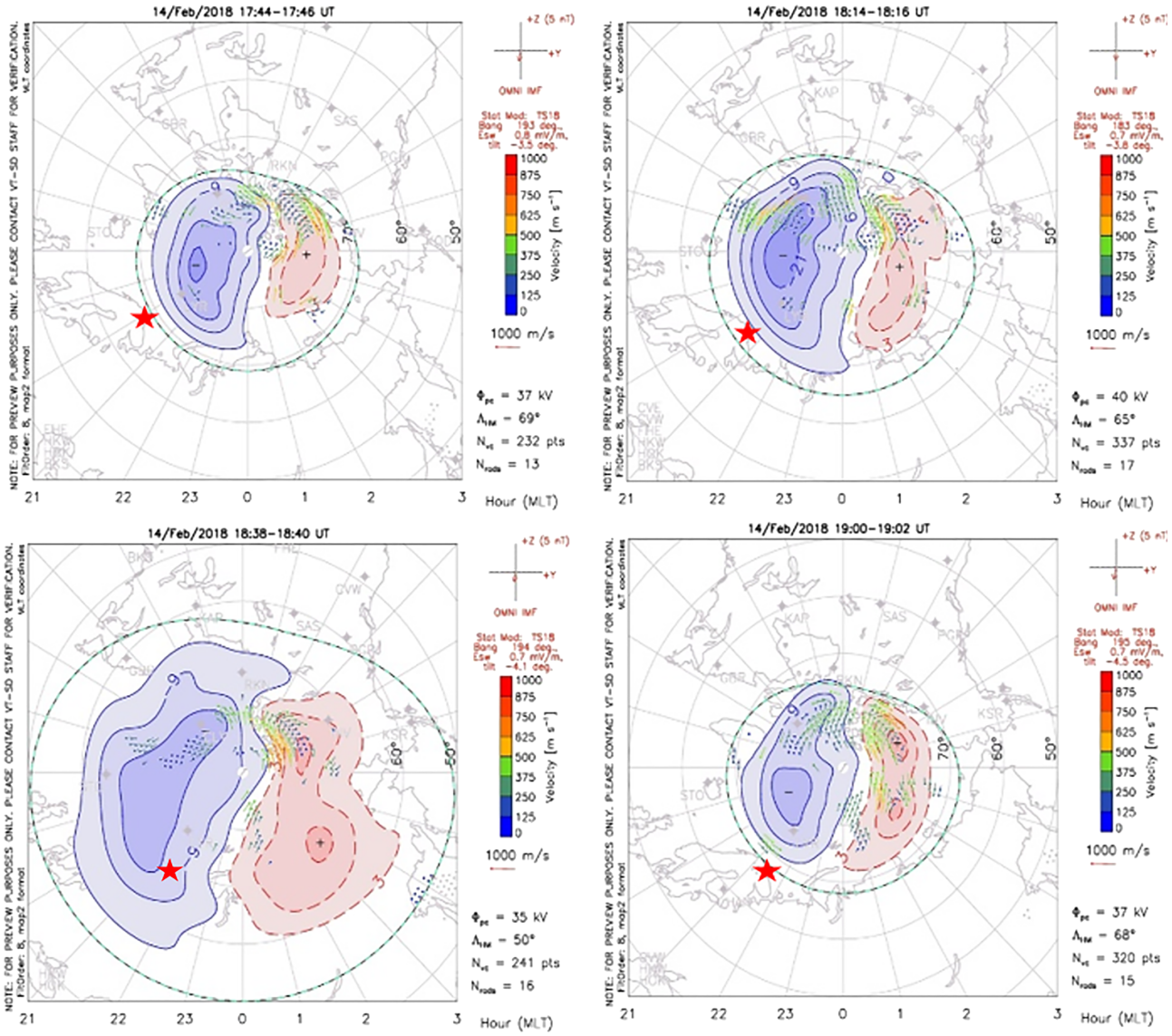

Figure 7. Representative convection maps during the time of eastward and westward moving MSTIDs for 14 February 2018. The approximate location of Tromsø is depicted by red mark.

field at Tromsø and Abisko. The positive increase in the X component implies the increase in the eastward Hall current in the E region. In the F region, both ions and electrons move in accordance with the $E \times B$ drift, causing no net flow of current (E and B are vectors of the electric and magnetic fields, respectively). However, the scenario gets changed in the E region where the ion-neutral collision frequency is higher than the ion gyrofrequency, causing relative motion of ions $(\overrightarrow{V}_i)$ and electrons $(\overrightarrow{V}_e)$ which, in turn, set up a current in the direction of $\overrightarrow{V}_i - \overrightarrow{V}_e$. Thus, it could be reasonably construed from the above discussion that the increase in the eastward Hall current in the E region corresponds to the westward $E \times B$ drift in the F region of the ionosphere due to poleward electric field. The presence of westward turning MSTIDs in conjunction with the simultaneous increase in the local X component suggests the crucial role of local electrodynamics in controlling the motion of MSTIDs.

The MSTIDs show persistent eastward propagation when there is no characteristic change in the X component of magnetic field at TRO and ABK (case 4). On the contrary, the MSTIDs continue to propagate in the westward direction when they occurred after the equatorward expansion of the auroral oval. The location of

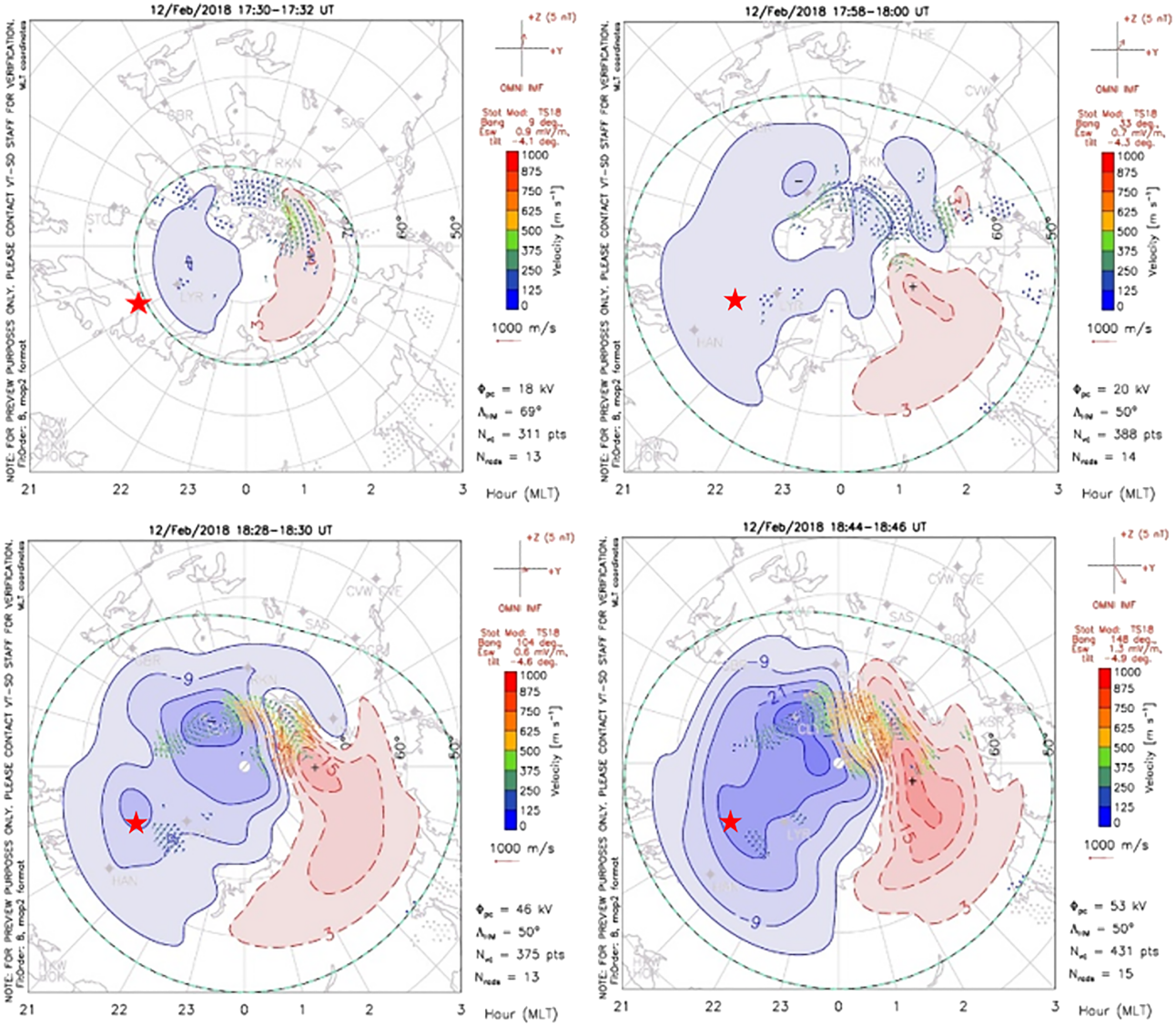

Figure 8. Same as Figure 7 but for 12 February 2018.

Tromsø was also found to be invariably inside or at the edge of the duskside high-latitude convection cell during the time of westward moving MSTIDs. The electric field in the equatorward side of the duskside auroral oval tends to be poleward, causing the westward drift of the ionospheric plasma in the two-cell convection pattern. Therefore, it is clear from the present observations that the auroral oval expands with increasing geomagnetic activity, causing Tromsø to come under the influence of westward convection electric fields. These results further imply that the observed MSTIDs are plasma structures and move in accordance with the background electric field as also pointed out by Shiokawa, Mori, et al. (2012).

Shiokawa, Mori, et al. (2012) explained the eastward drift of the MSTIDs over Tromsø by the *F* region dynamo driven by the eastward neutral wind. The *F* region dynamo (Rishbeth, 1971) with eastward neutral wind can cause eastward plasma drift in the ionosphere. Therefore, in order to understand the motion of MSTIDs, it is essential to examine the variation of horizontal neutral wind as it might play a role in controlling the motion of MSTIDs at high latitudes. The FPI measurements revealed that the neutral winds in the evening sector were dominantly eastward for the three cases and the westward acceleration of the wind was found to be associated with the enhanced geomagnetic activity. The pressure gradient created by the solar heating is the dominant force on the neutrals, causing the dominant eastward winds during the quiet

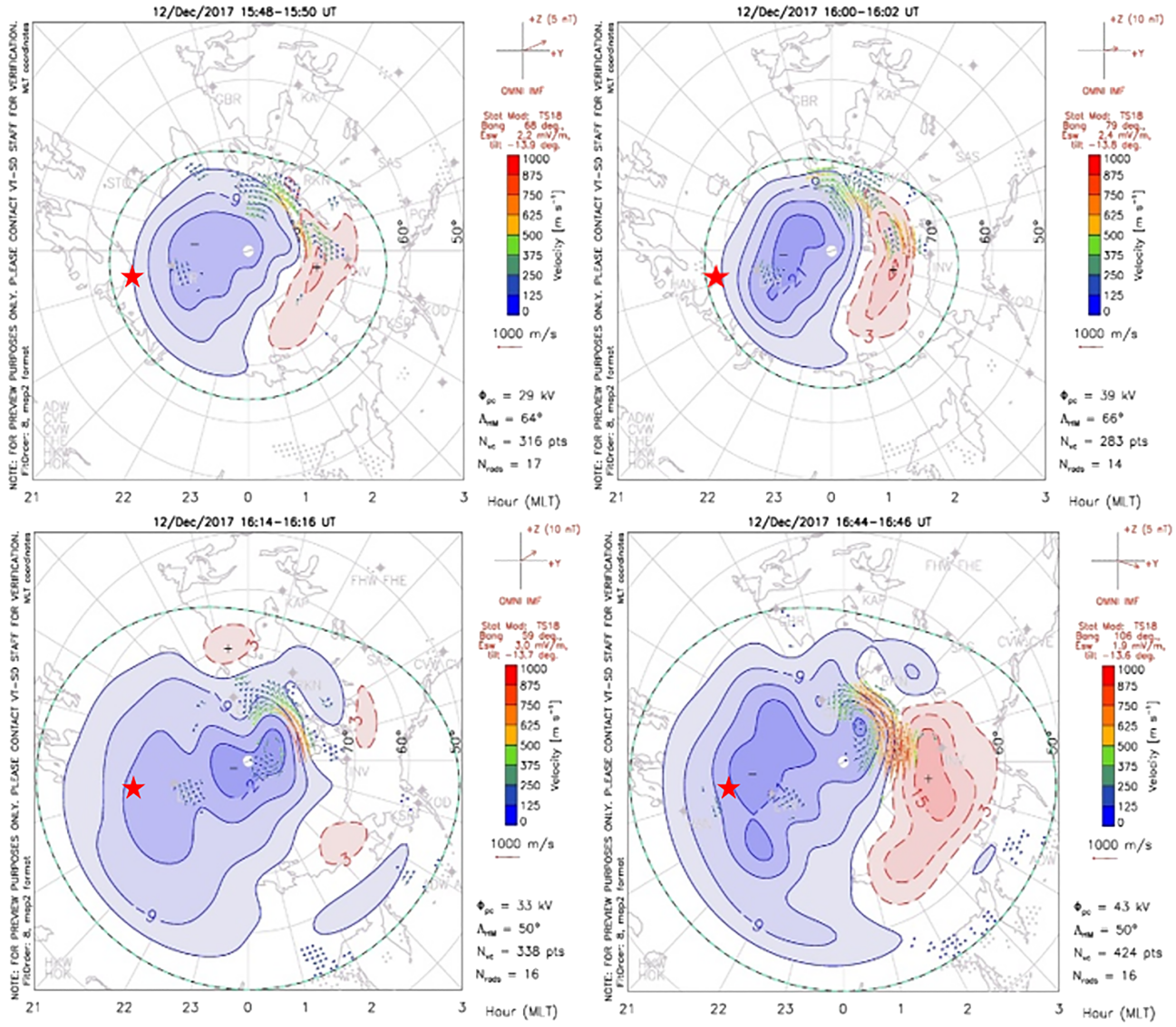

Figure 9. Same as Figure 7 but for 12 December 2017.

time in the dusk local-time sector. With increase in geomagnetic activity, the auroral oval intensifies and expands, causing neutrals to move in the direction of ion convection pattern which is westward in the dusk sector of the equatorward side of the auroral oval (e.g., Aruliah et al., 1999; Cai et al., 2019; Conde et al., 2001; Heppner & Maynard, 1987; Xu et al., 2019). The pressure-gradient driven eastward wind was accelerated westward with the intensification in the auroral activity. Using global ionosphere and thermosphere model, Wang et al. (2017) demonstrated that during the substorms the ion drag is a dominant force to produce the westward thermospheric winds in the duskside. It is worthy to note that in spite of the presence of aurora encompassing the entire region around Tromsø, the zonal wind remained in the eastward direction during 12 December 2017, although with a lesser magnitude as compared to the other two events. This could be associated with the fact that neutral particles take a finite time (an order of hours) to change their direction of motion caused by the ion motion through collisions.

4.2. Generation Mechanisms of MSTIDs

One of the most puzzling questions raised by the present results is the origin of the observed MSTID. The two major mechanisms, which are responsible for the generation of MSTIDs, are atmospheric gravity waves and

the ionospheric Perkins instability. Shiokawa, Mori, et al. (2012) speculated that MSTIDs over Tromsø could be originated in atmospheric gravity waves. Later, Shiokawa et al. (2013) by using lower atmospheric parameters at 250 hPa (~10 km) reported that the eastward and northeastward moving MSTIDs were caused by gravity wave source which was situated southwest of Tromsø. For the present case study, we have also analyzed the data of vertical pressure velocity, geopotential height, and local Rossby number (R0) to investigate the source region of the gravity waves that lead to the generation of MSTIDs. The analysis revealed (not shown here) the occurrence of large R0 mostly in the southward and westward direction of Tromsø with no favorable change in the set of vertical velocity and geopotential height. It should be noted here that the propagation of gravity waves from the troposphere to the thermosphere may be indirect. As the gravity waves propagate upward, that is, away from their source region, they undergo various filtering mechanisms. Depending upon their direction and phase velocity, they may either propagate up, or reflected back, or deposit their energy and momentum at the critical level. These gravity waves often undergo wave breaking phenomenon and produces secondary gravity waves with larger vertical scales and higher phase speeds (Fritts et al., 2011). These secondary waves, which are generated in the mesopause region, may serve as a direct cause of the MSTIDs (Vadas et al., 2003). Further, there may be a possibility of gravity wave source in the middle atmosphere or in the thermosphere. The gravity waves can also be generated in the thermosphere due to gradients caused by the solar terminator (Šauli et al., 2006).

The present observations show that MSTIDs respond to the electric field associated with auroral brightening and geomagnetic field perturbation. If the MSTIDs are generated by gravity waves, they should not respond to the electric field variation. We can consider that the plasma structure caused by gravity waves may move by the electric field. But in that case the phase front should reappear in the previous location expected from gravity wave motion, when the motion due to electric field variation ceases. However, in the present events, the phase front of MSTIDs moves back and forth continuously without any phase jump. These observations imply that MSTIDs do not have their origin in the gravity waves and plausibly generated by the plasma instability processes like the Perkins instability.

The Perkins instability plays an important role in the generation of MSTIDs over middle latitudes where they are known to propagate in the southwest direction in the Northern Hemisphere. The phase surface of these instabilities is aligned along NW-SE direction at middle latitudes (e.g., Shiokawa, Kadota, et al., 2003). The driving factor for triggering the MSTIDs in the midlatitudes is the presence of equatorward/southward wind (Perkins, 1973). In the present case, the FPI-derived wind was found to be predominantly northeastward. Note that FPI measurements were not made in the region of MSTIDs generation but correspond to the region of their propagation. Under the northeastward wind, it is a matter of great interest to investigate the role of Perkins instability in the development of MSTIDs. By studying the characteristics of nighttime MSTIDs using 630.0-nm airglow images obtained by ASI installed at Poker Flat Research Range, Kubota et al. (2011) argued that over Alaska, MSTIDs were generated by atmospheric gravity waves as they found the dominant northward neutral winds and westward plasma drifts during the appearance of MSTIDs. However, the instability caused by the change in the Pedersen conductance in the direction of the ionospheric currents can also play an important role in generating the Perkins instability (Perkins, 1973) through generation of polarization electric field and associated upward or downward motion of the ionosphere. The initial perturbation required to trigger such an instability can be formed by the small displacements of the electron density profile up and down along the magnetic field lines. Under the northward wind conditions which pushes the ionosphere down to the lower altitudes, if such perturbation is generated, it may trigger the instability (Makela & Otsuka, 2011).

In the observations under discussion, the northeastward thermospheric neutral wind ($\boldsymbol{u}$) generates northwestward ionospheric Pedersen current $J = \boldsymbol{\sigma_p}(\boldsymbol{E}+\boldsymbol{u} \times \boldsymbol{B})$, if E is enough smaller than $\boldsymbol{u} \times \boldsymbol{B}$ (case 1). Then the inhomogeneity in the conductivity generates a polarization electric field (E_p). For the Perkins instability to operate, the wave vector (k) of perturbation should lie in the NW or SE direction, because $\boldsymbol{u} \times \boldsymbol{B}$ is in the NW direction. This will give rise to NE-SW alignment of the phase surface of the MSTIDs. In the second case (case 2), if the magnetospheric electric field (E) is greater than $\boldsymbol{u} \times \boldsymbol{B}$, it could dominate the electrodynamics of the ionosphere. The poleward electric field in the equatorward side of the duskside auroral oval gives rise to the poleward ionospheric Pedersen current $J = \boldsymbol{\sigma_p}(\boldsymbol{E}+\boldsymbol{u} \times \boldsymbol{B})$, if $\boldsymbol{u} \times \boldsymbol{B}$ is smaller enough than the magnetospheric E. In this case, if the east-west component of E changes with time, the resultant k and phase surface would also change with time. The dominance of the magnetospheric E

might be a reason that the MSTIDs did not exhibit a uniform phase surface and displayed a tendency to change with time. These results plausibly imply that the Perkins instability triggered by magnetospheric *E* may be a favorable mechanism responsible for generating MSTIDs over high latitudes.

5. Conclusions

The propagation characteristics of duskside MSTIDs were studied by analyzing 630-nm airglow images, FPI-derived winds, SuperDARN derived convection maps, and magnetic field measurements at Tromsø and Abisko under various background conditions. The study is based on the five intriguing events of duskside MSTIDs observed over Tromsø. The scientific objective of this study is to investigate the background conditions under which duskside MSTIDs in the subauroral region exhibit a feature of rapid change in the propagation direction. Results suggest that the change in the propagation direction of duskside MSTIDs in the subauroral region is controlled by convection electric field. The westward turning of the MSTIDs is found to be associated with the local perturbations in the X component of the magnetic field and with the equatorward expansion of the auroral oval. Results suggest that variations in the local magnetic field are prerequisite to understand the role of local electrodynamics in controlling the dynamical structures in the *F* region of the ionosphere. While we do not have the direct measurements of the electric field for events selected in this study, the expansion of auroral oval and the brightening of aurora provide a reasonable clue to support an idea of intensification of the convection electric field. The intensified convection electric field appeared to result in westward turning of the duskside MSTIDs, which moved in the eastward direction during quiet geomagnetic conditions.

Acknowledgments
The optical data obtained at Tromsø are available through ISEE. Quick-look plots of the optical data are available at http://stdb2.isee.nagoya-u.ac.jp/omti/ website. The authors acknowledge the use of the convection mapping tool hosted by the Virginia Tech SuperDARN group at their website (http://vt.superdarn.org). The authors thank the institutes that maintain the IMAGE magnetometer array: Tromsø Geophysical Observatory of UiT the Arctic University of Norway (Norway). The baseline subtracted magnetic field data are available at the SuperMAG website (http://supermag.jhuapl.edu/). The solar wind parameters and geomagnetic indices were obtained from Space Physics Data Facility, NASA, USA (http://omniweb.gsfc.nasa.gov/ow_min.html). S. Y. duly acknowledges the Department of Science and Technology (DST) for the INSPIRE faculty award and director SPL for hosting the position. S. Y. also acknowledges NICT, Japan for giving fellowship under NICT International Exchange Program and ISEE, Nagoya University, Japan, for hosting the position. This work was supported by JSPS KAKENHI (15H05815, 15H05747, 16H02230, and 16H06286). A part of SO was supported by Academy of Finland (314664).

References

Amorim, D. C. M., Pimenta, A. A., Bittencourt, J. A., & Fagundes, P. R. (2011). Long term study of medium-scale traveling ionospheric disturbances using OI 630 nm all sky imaging and ionosonde over Brazilian low latitudes. *Journal of Geophysical Research*, *116*, A06312. https://doi.org/10.1029/2010JA016090

Aruliah, A. L., Müller-Wodarg, I. C. F., & Schoendorf, J. (1999). Consequences of geomagnetic history on the high-latitude thermosphere and ionosphere: Averages. *Journal of Geophysical Research*, *104*(A12), 28,073–28,088. https://doi.org/10.1029/1999JA900334

Bristow, W. A., Greenwald, R. A., & Samson, J. C. (1994). Identification of high-latitude acoustic gravity wave sources using the Goose Bay HF radar. *Journal of Geophysical Research*, *99*(A1), 319–331.

Cai, L., Oyama, S.-I., Aikio, A., Vanhamäki, H., & Virtanen, I. (2019). Fabry-Perot interferometer observations of thermospheric horizontal winds during magnetospheric substorms. *Journal of Geophysical Research: Space Physics*, *124*, 3709–3728. https://doi.org/10.1029/2018JA026241

Conde, M., Craven, J. D., Immel, T., Hoch, E., Stenbaek-Nielsen, H., Hallinan, T., et al. (2001). Assimilated observations of thermospheric winds, the aurora, and ionospheric currents over Alaska. *Journal of Geophysical Research*, *106*(A6), 10,493–10,508. https://doi.org/10.1029/2000JA000135

Fejer, B. G., & Kelley, M. C. (1980). Ionospheric irregularities. *Reviews of Geophysics*, *18*, 401–454.

Figueiredo, C. A. O. B., Takahashi, H., Wrasse, C. M., Otsuka, Y., Shiokawa, K., & Barros, D. (2018). Medium-scale traveling ionospheric disturbances observed by detrended total electron content maps over Brazil. *Journal of Geophysical Research: Space Physics*, *123*, 2215–2227. https://doi.org/10.1002/2017JA025021

Forbes, J. M., Bruinsma, S. L., Doornbos, E., & Zhang, X. (2016). Gravity wave-induced variability of the middle thermosphere. *Journal of Geophysical Research: Space Physics*, *121*, 6914–6923. https://doi.org/10.1002/2016JA022923

Fritts, D. C., Lund, T. S., & Hultqvist, B. (2011). Gravity wave influences in the thermosphere and ionosphere: Observations and recent modeling. In M. A. Abdu, & D. Pancheva (Eds.), *Aeron. Earth's atmos ionos* (Chap. 8, (pp. 109–130). Dordrecht: Springer. https://doi.org/10.1007/978-94-007-0326-1

Garcia, F. J., Kelley, M. C., Makela, J. J., & Huang, C.-S. (2000). Airglow observations of mesoscale low-velocity traveling ionospheric disturbances at midlatitudes. *Journal of Geophysical Research*, *105*, 18,407–18,415.

Garcia, R. F., Bruinsma, S., Massarweh, L., & Doornbos, E. (2016). Medium-scale gravity wave activity in the thermosphere inferred from GOCE data. *Journal of Geophysical Research: Space Physics*, *121*, 8089–8102. https://doi.org/10.1002/2016JA022797

Gjerloev, J. W. (2012). The SuperMAG data processing technique. *Journal of Geophysical Research*, *117*, A09213. https://doi.org/10.1029/2012JA017683

Hargreaves, J. K. (1992). *The solar-terrestrial environment* (p. 7). Cambridge: Cambridge University Press.

Heppner, J. P., & Maynard, N. C. (1987). Empirical high-latitude electric field models. *Journal of Geophysical Research*, *92*(A5), 4467–4489.

Hines, C. O. (1960). Internal atmospheric gravity waves at ionospheric heights. *Canadian Journal of Physics*, *38*(11), 1441–1481. https://doi.org/10.1139/p60-150

Hocke, K., & Schlegel, K. (1996). A review of atmospheric gravity waves and travelling ionospheric disturbances: 1982-1995. *Annales Geophysicae*, *14*, 917–940.

Huang, F., Lei, J., Dou, X., Luan, X., & Zhong, J. (2018). Nighttime medium-scale traveling ionospheric disturbances from airglow imager and Global Navigation Satellite Systems observations. *Geophysical Research Letters*, *45*, 31–38. https://doi.org/10.1002/2017GL076408

Hunsucker, R. D. (1982). Atmospheric gravity waves generated in the high-latitude ionosphere: A review. *Reviews of Geophysics*, *20*(2), 293–315. https://doi.org/10.1029/RG020i002p00293

Keskinen, M. J., & Ossakow, S. L. (1983). Theories of high latitude ionospheric irregularities. *Radio Science*, *18*, 1077.

Kotake, N., Otsuka, Y., Tsugawa, T., Ogawa, T., & Saito, A. (2007). Statistical study of medium-scale traveling ionospheric disturbances observed with the GPS networks in Southern California. *Earth, Planets and Space*, *59*, 95–102.

Kubota, M., Conde, M., Ishii, M., Murayama, Y., & Jin, H. (2011). Characteristics of nighttime medium-scale traveling ionospheric disturbances observed over Alaska. *Journal of Geophysical Research*, *116*, A05307. https://doi.org/10.1029/2010JA016212

Kubota, M., Shiokawa, K., Ejiri, M. K., Otsuka, Y., Ogawa, T., Sakanoi, T., et al. (2000). Traveling ionospheric disturbances observed in the OI 630-nm nightglow images over Japan by using a multi-point imager network during the FRONT campaign. *Geophysical Research Letters*, *27*(24), 4037–4040.

Makela, J. J., Miller, E. S., & Talaat, E. R. (2010). Nighttime medium-scale traveling ionospheric disturbances at low geomagnetic latitudes. *Geophysical Research Letters*, *37*, L24104. https://doi.org/10.1029/2010GL045922

Makela, J. J., & Otsuka, Y. (2011). Overview of nighttime ionospheric instabilities at low- and mid-latitudes: Coupling aspects resulting in structuring at the mesoscale. *Space Science Reviews*, *168*(1–4), 419–440. https://doi.org/10.1007/s11214-011-9816-6

Martinis, C., Baumgardner, J., Wroten, J., & Mendillo, M. (2010). Seasonal dependence of MSTIDs obtained from 630.0 nm airglow imaging at Arecibo. *Geophysical Research Letters*, *37*, L11103. https://doi.org/10.1029/2010GL043569

Martinis, C., Baumgardner, J., Wroten, J., & Mendillo, M. (2011). All-sky imaging observations of conjugate medium-scale traveling ionospheric disturbances in the American sector. *Journal of Geophysical Research*, *116*, A05326. https://doi.org/10.1029/2010JA016264

Narayanan, V. L., Shiokawa, K., Otsuka, Y., & Neudegg, D. (2018). On the role of thermospheric winds and sporadic *E* layers in the formation and evolution of electrified MSTIDs in geomagnetic conjugate regions. *Journal of Geophysical Research: Space Physics*, *123*, 6957–6980. https://doi.org/10.1029/2018JA025261

Nishioka, M., Saito, A., & Tsugawa, T. (2009). Super-medium-scale traveling ionospheric disturbance observed at midlatitude during the geomagnetic storm on 10 November 2004. *Journal of Geophysical Research*, *114*, A07310. https://doi.org/10.1029/2008JA013581

Oinats, A. V., Nishitani, N., Ponomarenko, P., Berngardt, O. I., & Ratovsky, K. G. (2016). Statistical characteristics of medium-scale traveling ionospheric disturbances revealed from the Hokkaido East and Ekaterinburg HF radar data. *Earth, Planets and Space*, *68*(1), 1–13. https://doi.org/10.1186/s40623-016-0390-8

Otsuka, Y., Shiokawa, K., Ogawa, T., & Wilkinson, P. (2004). Geomagnetic conjugate observations of medium-scale traveling ionospheric disturbances at midlatitude using all-sky airglow imagers. *Geophysical Research Letters*, *31*, L15803. https://doi.org/10.1029/2004GL020262

Otsuka, Y., Suzuki, K., Nakagawa, S., Nishioka, M., Shiokawa, K., & Tsugawa, T. (2013). GPS observations of medium-scale traveling ionospheric disturbances over Europe. *Annales Geophysicae*, *31*(2), 163–172. https://doi.org/10.5194/angeo-31-163-2013

Perkins, F. (1973). Spread *F* and ionospheric currents. *Journal of Geophysical Research*, *78*, 218–226.

Rishbeth, H. (1971). The *F*-layer dynamo. *Planetary and Space Science*, *19*, 263.

Ruohoniemi, M., & Baker, K. B. (1998). Large-scale imaging of high-latitude convection with super dual auroral radar network HF radar observations. *Journal of Geophysical Research*, *103*, 20,797–20,811.

Saito, A., Fukao, S., & Miyazaki, S. (1998). High resolution mapping of TEC perturbations with the GSI GPS network over Japan. *Geophysical Research Letters*, *25*, 3079–3082. https://doi.org/10.1029/98GL52361

Saito, A., Iyemori, T., Sugiura, M., Maynard, N. C., Aggson, T. L., Brace, L. H., et al. (1995). Conjugate occurrence of the electric-field fluctuations in the nighttime midlatitude ionosphere. *Journal of Geophysical Research*, *100*, 21,439–21,451. https://doi.org/10.1029/95JA01505

Šauli, P., Abry, P., Altadill, D., & Boska, J. (2006). Detection of the wave-like structures in the *F* region electron density: Two station measurements. *Studia Geophysica et Geodaetica*, *50*(1), 131–146. https://doi.org/10.1007/s11200-006-0007-y

Shiokawa, K., Ihara, C., Otsuka, Y., & Ogawa, T. (2003). Statistical study of nighttime medium-scale traveling ionospheric disturbances using midlatitude airglow images. *Journal of Geophysical Research*, *108*(A1), 1052. https://doi.org/10.1029/2002JA009491

Shiokawa, K., Kadota, T., Otsuka, Y., Ogawa, T., Nakamura, T., & Fukao, S. (2003). A two-channel Fabry-Perot interferometer with thermoelectric-cooled CCD detectors for neutral wind measurement in the upper atmosphere. *Earth, Planets and Space*, *55*(5), 271–275.

Shiokawa, K., Katoh, Y., Satoh, M., Ejiri, M. K., Ogawa, T., Nakamura, T., et al. (1999). Development of optical mesosphere thermosphere imagers (OMTI). *Earth, Planets and Space*, *51*, 887–896.

Shiokawa, K., Mori, M., Otsuka, Y., Oyama, S., & Nozawa, S. (2012). Motion of high-latitude nighttime medium-scale traveling ionospheric disturbances associated with auroral brightening. *Journal of Geophysical Research*, *117*, A10316. https://doi.org/10.1029/2012JA017928

Shiokawa, K., Mori, M., Otsuka, Y., Oyama, S., Nozawa, S., Suzuki, S., & Connors, M. (2013). Observation of nighttime medium-scale travelling ionospheric disturbances by two 630-nm airglow imagers near the auroral zone. *Journal of Atmospheric and Solar-Terrestrial Physics*, *103*, 184–194. https://doi.org/10.1016/j.jastp.2013.03.024

Shiokawa, K., Otsuka, Y., & Ogawa, T. (2009). Propagation characteristics of nighttime mesospheric and thermospheric waves observed by optical mesosphere thermosphere imagers at middle and low latitudes. *Earth, Planets and Space*, *61*, 479–491.

Shiokawa, K., Otsuka, Y., Oyama, S., Nozawa, S., Satoh, M., Katoh, Y., et al. (2012). Development of low-cost sky-scanning Fabry-Perot interferometers for airglow and auroral studies. *Earth, Planets and Space*, *64*(11), 1033–1046. https://doi.org/10.5047/eps.2012.05.004

Shiokawa, K., Otsuka, Y., Tsugawa, T., Ogawa, T., Saito, A., Ohshima, K., et al. (2005). Geomagnetic conjugate observation of nighttime medium-scale and large-scale traveling ionospheric disturbances: FRONT3 campaign. *Journal of Geophysical Research*, *110*, A05303. https://doi.org/10.1029/2004JA010845

Sivakandan, M., Chakrabarty, D., Ramkumar, T. K., Guharay, A., Taori, A., & Parihar, N. (2019). Evidence for deep ingression of the midlatitude MSTID into as low as ~3.5° magnetic latitude. *Journal of Geophysical Research: Space Physics*, *124*, 749–764. https://doi.org/10.1029/2018JA026103

Ssessanga, N., Kim, Y. H., & Jeong, S.-H. (2017). A statistical study on the *F*2 layer vertical variation during nighttime medium-scale traveling ionospheric disturbances. *Journal of Geophysical Research: Space Physics*, *122*, 3586–3601. https://doi.org/10.1002/2016JA023463

Tanskanen, E. I. (2009). A comprehensive high-throughput analysis of substorms observed by IMAGE magnetometer network: Years 1993-2003 examined. *Journal of Geophysical Research*, *114*, A05204. https://doi.org/10.1029/2008JA013682

Tsugawa, T., Otsuka, Y., Coster, A. J., & Saito, A. (2007). Medium-scale traveling ionospheric disturbances detected with dense and wide TEC maps over North America. *Geophysical Research Letters*, *34*, L22101. https://doi.org/10.1029/2007GL031663

Vadas, S. L., Fritts, D. C., & Alexander, M. J. (2003). Mechanism for the generation of secondary waves in wave breaking regions. *Journal of the Atmospheric Sciences*, *60*(1), 194–214. https://doi.org/10.1175/1520-0469(2003

Virginia Tech SuperDARN group (2015). Convection map plotting on-line tool. << ENTER APPROPRIATE URL HERE >>Accessed on DAY - MONTH - YEAR

Wang, H., Zhang, K. D., Wan, X., & Lühr, H. (2017). Universal time variation of high-latitude thermospheric disturbance wind in response to a substorm. *Journal of Geophysical Research: Space Physics*, *122*, 4638–4653. https://doi.org/10.1002/2016JA023630

Xu, H., Shiokawa, K., Oyama, S., & Otsuka, Y. (2019). Thermospheric wind variations observed by a Fabry-Perot interferometer at Tromsø, Norway, at substorm onsets. Earth. *Planets and Space*, *71*(1), 1–13. https://doi.org/10.1186/s40623-019-1072-0

Yokoyama, T., & Hysell, D. L. (2010). A new midlatitude ionosphere electrodynamics coupling model (MIECO): Latitudinal dependence and propagation of medium-scale traveling ionospheric disturbances. *Geophysical Research Letters*, *37*, L08105. https://doi.org/10.1029/2010GL042898

Yokoyama, T., Hysell, D. L., Otsuka, Y., & Yamamoto, M. (2009). Three-dimensional simulation of the coupled Perkins and *Es*-layer instabilities in the nighttime midlatitude ionosphere. *Journal of Geophysical Research*, *114*, A03308. https://doi.org/10.1029/2008JA013789